THE JOURNAL OF PHYSICAL CHEMISTRY A

pubs.acs.org/JPCA Article

# Singlet Fission Dynamics in Tetracene Single Crystals Probed by Polarization-Dependent Two-Dimensional Electronic Spectroscopy

*Published as part of The Journal of Physical Chemistry virtual special issue "Josef Michl Festschrift".*

Guodong Wang, Chunfeng Zhang,* Zhixing Liu, Rui Wang, Haibo Ma, Xiaoyong Wang, and Min Xiao

Cite This: *J. Phys. Chem. A* 2020, 124, 10447−10456 Read Online



**ABSTRACT:** The exact mechanism of endothermic singlet fission in crystalline polyacene remains to be clarified. It has been elusive whether the excess energy of vibrational hot states and the upper branch of Davydov splitting is important for the energy compensation. Here, we probe the excited-state specified singlet fission dynamics in tetracene single crystals by polarization-dependent two-dimensional electronic spectroscopy (2DES). While a major spectral transfer with a characteristic lifetime of 86 ps is observed to be largely independent of the excitation energy due to formation of the spatially separated triplet pairs ($^1$(T···T)), the excitation-energy dependent subpicosecond dynamics show marked differences for different states probed, implying the possible involvement of a coherently formed triplet pair state ($^1$(TT)). Analysis of coherent vibrational modes suggests the coupling to high energy modes may offset the energy difference between singlet and triplet pair states. Moreover, the beating map of the low frequency mode indicates a vibrational hot state violating the aggregation behavior of Davydov exciton, which can be explained as a resonance of the $^1$(TT) state. These results suggest that the coherent vibronic mixing between local excitation and triplet pair states is essential for the singlet fission dynamics in molecule aggregates.

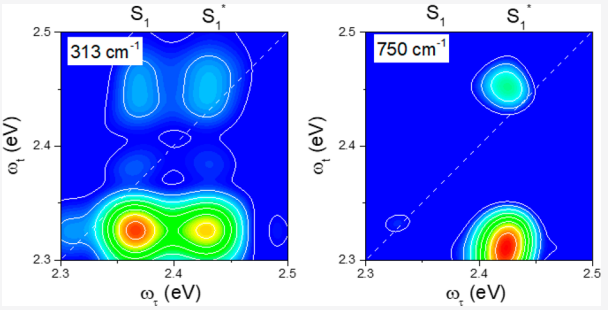


## INTRODUCTION

Singlet fission (SF) is a spin-allowed process that converts a photogenerated spin-singlet exciton ($S_1$) into a pair of triplet excitons ($T_1$ + $T_1$) in organic chromophores.[1−6] Benefiting from the multiplication of photoexcited charges, SF can potentially break the Shockley−Queisser limit in singlet-junction photovoltaic devices.[7−9] In the past decade, highly efficient SF has been observed in multiple molecule systems.[10−12] SF efficiency is high not only in the exothermic systems ($E(S_1) > 2E(T_1)$) like pentacene and derivatives[13−15] but also in many endothermic systems ($E(S_1) < 2E(T_1)$) including tetracene, rubrene and their derivatives.[16−26]

An intermediate state of a correlated triplet pair state[1−3,27,28] ($^1$(TT)) has been widely accepted to elucidate the SF mechanism, i.e., $S_1 \longleftrightarrow {}^1(TT) \longleftrightarrow T_1 + T_1$. The $^1$(TT) state is possibly formed by direct electronic coupling between $S_1$ and $^1$(TT) or through an indirect channel mediated by a charge-transfer (CT) state.[27,29−37] The triplet pair state is further dissociated into free triplets ($T_1$ + $T_1$). Such a scenario can well explain most aspects of SF dynamics. Nevertheless, in endothermic systems, the mechanism for overcoming the energy barrier remains elusive. Previous works suggest that the energy barrier can be compensated by the excess energy of vibrationally hot excitons provided by optical excitation in tetracene and anthracene.[16−19,38,39] It was proposed that direct SF from the higher-lying singlet states $S_n$ may proceed on a subpicosecond time scale, while the thermalized $S_1$ state precedes SF on a longer time scale of tens of picoseconds in the tetracene film.[16,17,19] Recently, optical spectroscopic data have suggested that endothermic SF is driven by spatial separation of the correlated triplet pair ($(^1(T_1T_1) \rightarrow {}^1(T_1\cdots T_1)$) which is formed coherently with the $S_1$ state upon optical excitation on an ultrafast time scale in the films of rubrene and TIPS−tetracene.[40,41]

The early stage dynamics of $^1$($T_1T_1$) state is primarily determined by the electronic couplings among the local excited singlet (LE), the CT and the $^1$($T_1T_1$) states.[15,29,37,38,40−45] In the systems such as tetracene and rubrene with weak direct electronic couplings, exciton−vibration couplings are essential for coherent formation of the $^1$($T_1T_1$) state.[38,41,46−50] The intramolecular modes coupled to the LE, CT, and/or TT states may strongly modulate the site energies toward energy

Received: September 16, 2020
Revised: November 18, 2020
Published: December 8, 2020







https://dx.doi.org/10.1021/acs.jpca.0c08440
J. Phys. Chem. A 2020, 124, 10447−10456

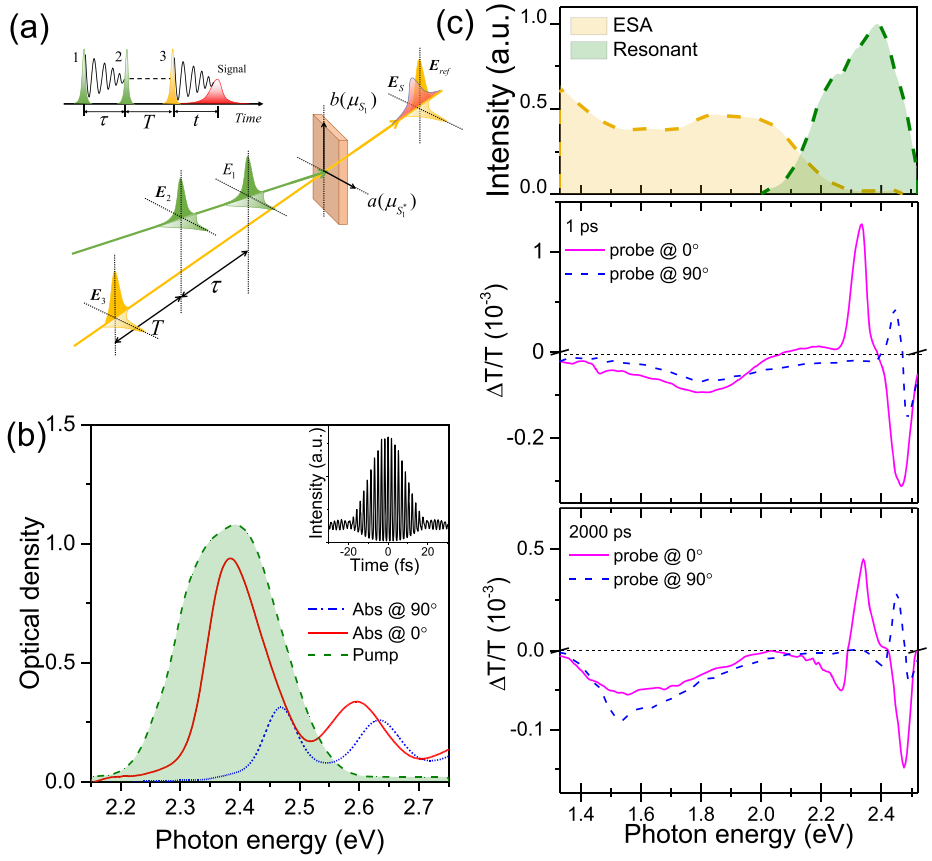


**Figure 1.** (a) Schematic diagram of polarization-dependent 2DES setup in the pump−probe geometry. The polarization angles of 0° and 90° represent the beam polarizations in parallel and perpendicular to the *b* axis of the tetracene crystal, respectively. (b) Absorption spectra of the single crystal tetracene sample with incident light polarized parallel and perpendicular to the *b* axis, corresponding to the transitions from ground $S_0$ to the $S_1$ and $S_1$* states arising from Davydov splitting. The spectrum of the pump beam is included for comparison. Inset shows the FRAC curve of the incident pulse. (c) Spectra of probe beams used in the 2DES experiments shown in comparison with the TA spectra recorded at the delay of 1 and 2000 ps with probe beam polarized parallel and perpendicular to the *b* axis of the crystal.

resonances.[46,51] The transformation of coherent phonon modes during $S_1 \rightarrow {}^1(T_1T_1)$ has been experimentally observed by two-dimensional electronic spectroscopy (2DES).[43] Alternatively, the nonlocal vibrational coupling with some intermolecular modes causes the symmetry breaking that may enhance the electronic couplings between these electronic states.[38,52−54] Such an effect is probably responsible for the SF rate promoted by selective phonon excitation in tetracene films with shaped pump pulses and the phonon mode transfer during $S_1 \rightarrow {}^1(T_1T_1)$ in rubrene.[55]

The dipole−dipole interaction in the molecule aggregates further complicates the energetic landscape for the excited species of LE, CT, and/or TT states.[56] In the acene crystals with inequivalent molecules in a unit cell, the Davydov splitting shifts the lowest singlet transition to both lower ($S_1$) and higher energy sides ($S_1$*) depending on excitation polarization.[12,57,58] Nevertheless, whether and how the upper Davydov branch, the vibrational hot states, and the interplay between these excited states affect the coherent exciton dynamics remain unclear. The issue is partially caused by the difficulties in elucidating the triplet generation dynamics triggered by transitions to specific excited states.

In this work, we try to tackle this issue with polarization-dependent 2DES with selective excitations of $S_0 \rightarrow S_1$ and $S_0 \rightarrow S_1$* transitions in tetracene crystals (Figure S1). 2DES encodes real-time correlations between the energies of the states photoexcited and probed,[59−61] which allows one to probe SF dynamics with high temporal resolution and excitation energy resolution simultaneously.[40,62] The experimental data suggest that in addition to the formation of ${}^1(T\cdots T)$ within 86 ps, the subpicosecond exciton dynamics show marked dependence on the excitation energy. The oscillations entangled in the dynamics suggest the high energy modes coupled to the singlet and triplet pair states may compensate the energy differences. Moreover, the beating map of low frequency mode indicates a vibrational hot state violating the aggregation behavior of Davydov exciton which can be explained as a resonance of the ${}^1(TT)$ state. These results suggest the coherent vibrations may give rise to mixing between the LE and triplet pair states which is essential for the SF dynamics in molecule aggregates.

## METHODS

We conducted polarization-dependent 2DES experiments to study the exciton dynamics in tetracene crystals. 2DES records the third-order nonlinear optical response of three sequenced pulses.[63−65] As described in a previous method paper, our setup of 2DES is configured in a pump−probe geometry.[66] The two collinear pump pulse replicas were created using a Mach−Zehnder interferometer with phase stabilized by active


https://dx.doi.org/10.1021/acs.jpca.0c08440
J. Phys. Chem. A 2020, 124, 10447−10456

feedback electronics. Such a configuration allows us to independently detune the pump−probe polarization configuration. (Figure 1a). A 5 kHz Ti:sapphire regenerative amplifier (Libra, Coherent) emitting at 800 nm with the pulse duration of ∼90 fs was employed to generate the pump and probe sources. The pump beam was generated by a homemade noncollinear optical parametric amplifier (NOPA) with the spectrum covering the absorption peaks of the transitions from $S_0$ to $S_1$ and $S_1$* states in the tetracene crystal (Figure 1b). To obtain good temporal resolution, the pump pulses were compressed by combining a pair of chirp mirrors and a pair of silica wedges. The overall pulse duration was ∼15 fs (Inset, Figure 1b) which was characterized by the fringe-resolved autocorrelator (FRAC) method. The probe beam was divided into two parts (Figure 1c) using another NOPA to cover the near resonance regime and using supercontinuum light to cover the long-wavelength range by focusing the output beam at 1300 nm from a homemade OPA onto a 3 mm sapphire plate. The probe pulse was also compressed by a pair of chirp mirrors together with silica wedges pairs. The spectra of transmitted probe beams ($T(\lambda)$) were analyzed by a CMOS camera mounted on a monochromator (Acton SP-2358, Princeton Instruments). Transmitted light ($T(\lambda)$) is probed with pulse-to-pulse spectral analysis at 5 kHz enabled by a homemade field programmable gate array (FPGA) control board. Using the heterodyne detection, the field of nonlinear optical response was calculated with the signal of $\Delta T/T^{0.5}$ where T is the transmitted probe light and $\Delta T$ is the pump-induced change. The $\tau$ scan range is from −150 to +150 fs. Fluence-dependent experiments were conducted (Figure S2). The 2DES data recorded with weak excitation with fluence of 5 $\mu J/cm^2$ are presented for illustrating the exciton dynamics while the oscillation components are obtained from the data recorded with excitation fluence of 100 $\mu J/cm^2$. In this work, the pulse consequence was set for recording the absorptive 2DES data. Optical measurements were conducted at room temperature.

The samples of tetracene single crystals were grown using the method of physical vapor deposition in a quartz tube.[67] The vapor of tetracene was carried by the argon flow (25 sccm) and then deposited onto substrates in the crystal growth zone. The sizes and thicknesses of the crystals were controlled by the amount of powder source and the growth time. We selected the single crystals with thickness of ∼300 nm and size up to 2 × 2 $mm^2$ and transferred the crystals on copper wire grids for 2DES measurements.[17]

Tetracene crystal has a layered, herringbone structure. Due to molecular interaction, the lowest excited state is split into two excitonic states $S_1$ and $S_1$*, i.e., the Davydov splitting.[57,58] The transition dipole from the ground state $S_0$ to $S_1$ state is nearly parallel to the *b* axis while the transition dipole from $S_0$ to $S_1$* state is nearly perpendicularly to the *b* axis. The absorption spectrum of the tetracene single crystal shows strong polarization dependence (Figure 1b), which allows selectively exciting the $S_1$ and $S_1$* states with different polarized pump configuration. The lower and upper Davydov branches, i.e., the transitions from the $S_0$ to the $S_1$ and $S_1$* states, show J-aggregate and H-aggregate-like behaviors.[56,58,68] The vibronic progressions are also manifested with absorption peaks in the higher energy region.[57,69] The polarization effect is also distinct in the excited state dynamics. As shown in Figure 1c, the bleach signals in the near resonance regime are highly polarized. In addition, the excited-state absorption (ESA) features for the transitions from the singlet and triplet excited states are also dependent on the probe polarization (Figure 1c). In the long-wavelength range, the singlet-related and triplet-related ESA features at 1.86 and 1.54 eV are partially polarized parallel and perpendicular to the *b* axis, respectively.

## RESULTS AND DISCUSSION

Figure 2 shows the typical 2DES data recorded at the different population delays with parallel pump to excite the transition of $S_0 \rightarrow S_1$. With a parallel probe, the positive signal appears with the probe energy at 2. 32 eV slightly below the $S_1$ transition, which can be ascribed to the ground-state bleach (GSB) and stimulated emission (SE) of 0−0 vibronic transition. Upon optical pump, negative signals are observed at the early stage with a sharp spectral feature centered at probe energy of 2.45 eV and a broad feature centered at 1.86 eV. These signals have been assigned to the ESA of singlet states. In addition, weak positive signal can be captured in the range of 2.1−2.25 eV which is caused by the SE of the vibronic replica. With a perpendicular probe, the positive signal is observed with probe energy at 2.46 eV due to the GSB of $S_0 \rightarrow S_1$* state. Following the decay of the initially photoexcited signal, spectral transfer is observed with an additional negative feature with the parallel probe at 2.28 eV and a broad negative feature with the perpendicular probe centered at 1.54 eV. These new ESA features have been assigned to the $T_1$ state and TT pair state in literatures.[16,21,70] Similar features of SF dynamics have also been observed in the 2DES data recorded with perpendicular excitation (Figure S3). Notably, the ESA features in the near resonance spectral range are entangled with the GSB features, making it very difficult to clearly assign it to specific transitions.

The spectral transfer of exciton dynamics in the tetracene crystal is more distinct in the sliced spectra (Figure 3). In the low energy regime, the ESA feature at 1.86 eV decreases markedly while the feature in the range of <1.6 eV remains nearly unchanged with probe polarization aligned parallel to the *b* axis (Figure 3a). In contrast, the signal with perpendicular probe shows an increase in the spectral range centered at 1.54 eV (Figure 3b). The ESA feature centered at 1.86 eV emerges simultaneously upon optical excitation and exhibits decay dynamics similar to PL decay, which has been widely accepted as the ESA feature for $S_1 \rightarrow S_n$ (Figure S4, Supporting Information).[16,21,70] The ESA signal for the transitions $S_1 \rightarrow S_n$ and $TT_1 \rightarrow TT_n$ are centered at 1.86 and 1.54 eV with some spectral overlap, which are partially polarized parallel and perpendicular. These results allow us to adopt the dynamics recorded at 1.86 eV with parallel probe and 1.54 eV with perpendicular probe to describe the singlet and triplet dynamics. The entangled ESA features of the singlet and triplet species with different dependences on probe polarization are responsible for the polarization-dependent spectral bandwidths (Figure 3). Upon $S_0 \rightarrow S_1$ excitation, the major spectral transfer occurs with a lifetime parameter of ∼86 ps (Figure 4) which agrees well with literature results.

To study the possible effects of vibrationally hot states and the upper branch of Davydov states, we compare the dynamics with different excitation energies and polarizations. As shown in Figure 4, the kinetics probed at different characteristic energies are nearly the same on the time scale longer than 1 ps. Regardless of the excitation energy, the major part of the spectral transfer occurs on the time scale of 86 ps, which was quoted as the SF rate and more specifically the buildup of $^1(T_1...T_1)$ states. Previously, the $^1(T_1T_1)$-liked multiexciton


https://dx.doi.org/10.1021/acs.jpca.0c08440
J. Phys. Chem. A 2020, 124, 10447−10456

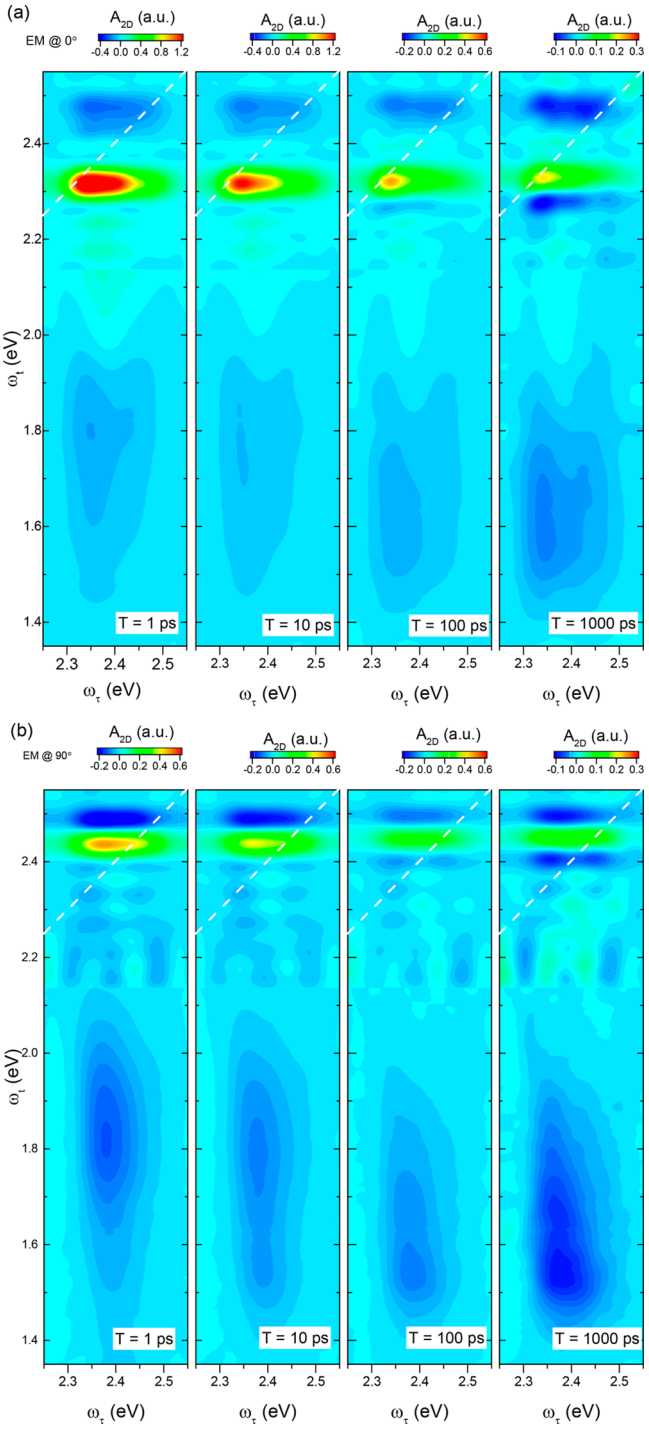


**Figure 2.** Absorptive 2DES spectra recorded from the tetracene crystal at different population delays with probe beam polarization (a) parallel and (b) perpendicular to the *b* axis of the crystal. The polarization of the excitation beam is parallel to the *b* axis.

states were identified by photoelectron emission spectroscopy in the tetracene films by Zhu et al.[34] Nevertheless, direct optical spectroscopic evidence has been inadequate in the tetracene film, which is possibly due to the mixing of LE and TT states in the nonadiabatic states involved in the optical transitions. The mixed transient absorption (TA) signals of these excited states make it challenging to fully separate their characteristic spectral features. Previously, the fast onset of the ESA signal probed near 1.5 eV in the TA data was assigned to the coherent formation of triplet signal due to direct conversion from vibrationally hot states. In the tetracene crystal, it was also suggested that the higher level $S_1$* may undergo a faster SF process with a smaller energy gap between $S_1$* and TT states by assuming the ESA signal of triplet pair state in the near resonance spectral range. To study the possible involvement of $^1(T_1T_1)$ state, we focus on the subpicosecond dynamics, which show marked differences on the excitation configurations. For the GSB signal with the probe energy at 2.32 eV (Figure 4a), delayed rising behaviors are distinct on the earliest 0.5 ps for above $S_1$ excitations of both parallel and perpendicular polarizations. Such delayed rise behaviors are also observed in the SE kinetics (Figure 4b). Notably, the kinetics with different polarized excitations at 2.45 eV show similar kinetics and spectral features (Figure 3). The signals are caused by the thermal relaxation to the $S_1$ state from these higher excited states of both vibrationally hot states and higher branch of Davydov states. Nevertheless, such dynamics related to the thermal relaxation are not observed in the kinetics probed at 1.86 eV (Figure 4c) and 1.54 eV (Figure 4d). The onset of the signals probed at 1.54 eV are nearly independent of excitation energy, implying the absence of additional SF channel from vibrationally hot states. The early stage dynamics probed at 1.86 eV are similar for both of $S_0 \rightarrow S_1$ and $S_0 \rightarrow S_1$* excitations. These results suggest the formation of an excited state prior to the thermal relaxation with the characteristics of singlet and triplet ESA features. In analogy to early studies, we speculate that this is a signature of coherently formed LE and $^1(T_1T_1)$ states. The decoherence between these LE/ $^1(T_1T_1)$ states may contribute to the slight increase of the signals probed at 1.54 eV (Figure S5). The spatial separation of $^1(T_1T_1) \rightarrow {}^1(T_1 \cdots T_1)$ states may further drive the SF generation, leading to the spectral transfer with the characteristic lifetime of 86 ps.

As the electronic couplings between LE and $^1(T_1T_1)$ states are very weak, the coherence, if there is any, is probably generated from vibronic mixing. We carefully analyze the oscillations entangled on the dynamic curves (Figures S6 and S7). Figure 5 compares the oscillation parts in the traces probed at different energies with $S_0 \rightarrow S_1$ and $S_0 \rightarrow S_1$* excitations. For both excitations, higher frequency modes (1160 $cm^{-1}$, 1200 $cm^{-1}$, 1384 $cm^{-1}$) are observed in the traces for the signals with parallel probe at 1.86 eV (Figure 5, parts e, f, m, and n) and perpendicular probe at 1. 54 eV (Figure 5, parts g, h, o, and p) with different intensity ratio. Similar behaviors are also observed for the traces of SE signals probed at 2.18 eV (Figure 5, parts c, d, k, and i). During the conversion of LE $\rightarrow {}^1(T_1T_1)$ state, these high frequency modes are probably coupled with the potential energy surface of the LE $\rightarrow {}^1(T_1T_1)$ states, respectively.[45] These modes are efficient to compensate the energy differences between the excited species. No significant difference is observed in the line widths and frequencies of these modes during the conversion, implying these modes are not strongly coupled to the reaction coordinates. Moreover, the amplitudes of the oscillation components are generally less than 5% of total amplitudes of the ESA signals, implying the coherent process is possibly responsible for part of the SF process.[71] A large portion of $^1(T_1 \ldots T_1)$ population may be generated from the relaxed $S_1$ state from an incoherent manner.[72]

Notably, the oscillation components in the GSB dynamics shows marked differences with $S_0 \rightarrow S_1$ and $S_0 \rightarrow S_1$* excitations especially for the low frequency modes. For the


https://dx.doi.org/10.1021/acs.jpca.0c08440
J. Phys. Chem. A 2020, 124, 10447−10456

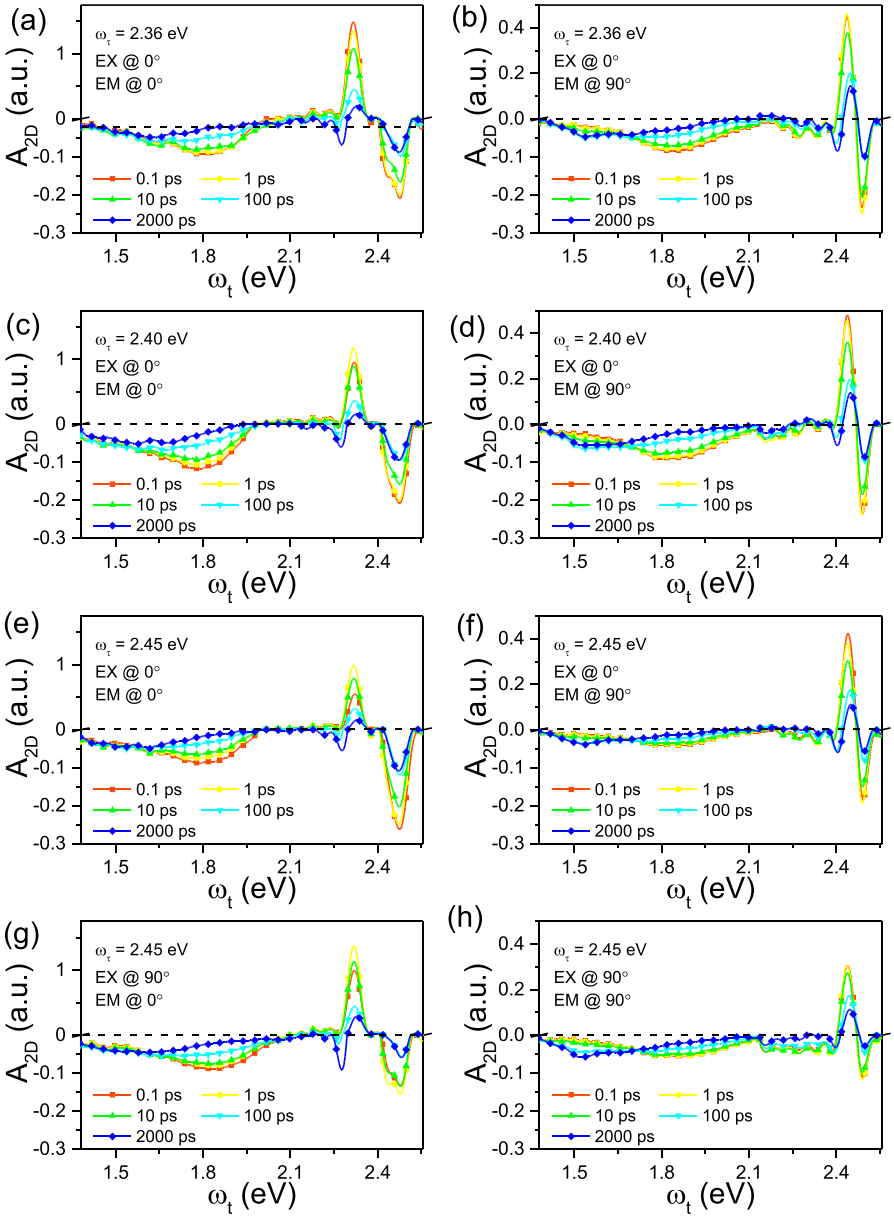


**Figure 3.** Sliced 2D spectra recorded at different population delays with different pump configurations. EX and EM stand for the excitation and probe polarizations, respectively.

GSB signal related to the $S_0 \rightarrow S_1$ transition, the modes of 131 and 313 $cm^{-1}$ are particularly pronounced. In addition to these two modes, the modes of 617 and 750 $cm^{-1}$ are also distinct in the GSB trace with $S_0 \rightarrow S_1$* excitation. Since these modes are all coupled to the ground state as characterized by Raman spectroscopy (Figure S8), these differences are possibly due to the aggregation behaviors of these transitions. In theory, the 0−1 vibronic transitions are markedly different for H- and J-aggregates.[56] For a J-aggregation dominated systems, 0−1 transition is markedly suppressed. In the tetracene crystal, the optical transitions are mainly related to the hybrid H- and J-aggregation behavior for the upper and lower Davydov branches.[22,56,58,68] For the parallel excitation, the J-aggregation prohibits the 0−1 transitions for the modes of 617 and 750 $cm^{-1}$ due to certain symmetry factors, which probably explains the different oscillation behaviors in the GSB for the $S_0 \rightarrow S_1$ and $S_0 \rightarrow S_1$* transitions. These results also imply that the aggregation effects may be markedly different for the vibronic transitions related to different vibrational modes. For more insight about the aggregation effect on the exciton−vibrational coupling, we survey the electron−phonon interaction in two different configurations of tetracene dimers in the single crystals (Figure S1, Supporting Information, for details).[46,52] In the dimers, both deformation modes of 617 and 750 $cm^{-1}$ displays the symmetric and asymmetric modes of vibrations (Figures S9−S11, Supporting Information). The computational results suggest that the coupling between the low-lying $S_1$ state to these modes, especially for the asymmetric vibrations, is significantly reduced in the dimer if compared to the monomer (Tables S2−S4). These results suggest that the nonlocal electron−phonon coupling plays an important role for the coherent vibrational dynamics in the tetracene aggregates.[73,74]



https://dx.doi.org/10.1021/acs.jpca.0c08440
J. Phys. Chem. A 2020, 124, 10447−10456

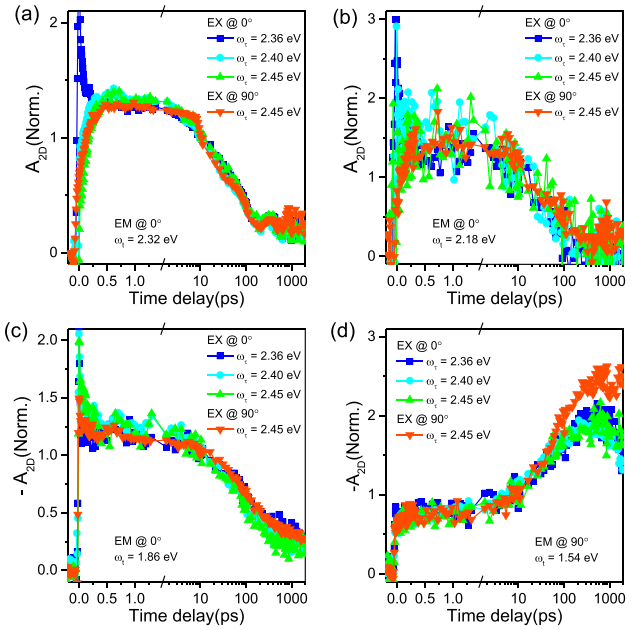


**Figure 4.** Temporal dynamics recorded from 2DES at different pump energies ($\omega_\tau$) and polarizations. The traces are recorded with probe energies at (a) 2.32, (b) 2.18, and (c) 1.86 eV with parallel probe polarization and (d) 1.54 eV with perpendicular probe polarization, respectively. The traces are normalized with the values recorded at the population delay of 10 ps.

The excitation-dependent coherent vibrational behavior is also manifested in the parallel excitations of different energies. Parts a and b of Figure 6 compare the beating amplitude in the 2D map for the modes of 313 and 750 $cm^{-1}$ with parallel excitation and probe polarizations. In addition to the resonance near $S_0 \rightarrow S_1$ transition, pronounced beating behaviors are observed for the excitation energy at 2.42 eV. Notably, the mode of 750 $cm^{-1}$ is also distinct with excitation energy at 2.42 eV like that of $S_0 \rightarrow S_1$* transition (Figure 6c). Parts d and e of Figure 6 show the spectra of beats at different modes recorded at the GSB feature at 2.32 eV and the ESA feature at 2.46 eV with the 2D signal as a reference. These data suggest there is a resonance near 2.42 eV with beating behavior dramatically different from that of $S_1$ state. As the resonance is observed with different modes, we can safely exclude its origin of a vibronic replica of specific vibrational mode. We labeled such a state as $S_1'$ in the following discussion. The excitation pathway for the beating in the GSB kinetics can be described in Figure 6f. When the excitation levels of $S_1'$ and $S_1$ are the same, the beating appears at the near diagonal as the beating modes of 131 and 313 $cm^{-1}$. As the modes probed in the signal with the excitation at 2.42 eV, the right channel should be excluded, which suggests an efficient coupling between the $S_1$ state and the vibrational mode. Otherwise, the beating signal should be distinct in the diagonal signal for the $S_0 \rightarrow S_1$ state. For parallel excitations, the transition at 2.42 eV was naturally assigned to the vibrational hot states of $S_1$ with J-aggregation behavior. The dynamics of 2D signal and the oscillation components are analyzed with excitation at 2.42 eV in Figure S7, which is markedly different from the $S_0 \rightarrow S_1$ transition. The different beating behavior implies the $S_1'$ transition is different from J-aggregation behavior. Considering a binding energy of $^1(T_1T_1)$ state of 100 meV,[5] the $S_1'$ energy is very close to that of

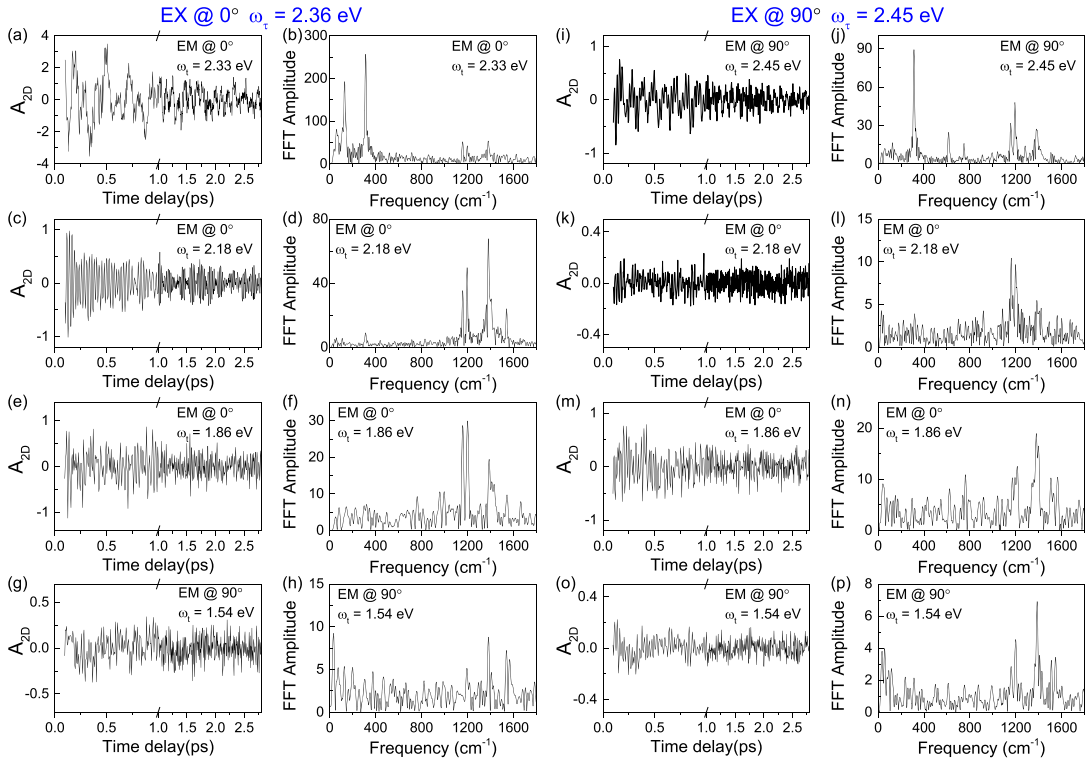


**Figure 5.** Oscillation components extracted from the dynamic curves and the Fourier transform spectra probed at different energies and polarizations with selective excitations at $S_0 \rightarrow S_1$ and $S_0 \rightarrow S_1$* transitions with (a–h) a parallel pump at 2. 36 eV and (i–p) a perpendicular pump at 2.45 eV, respectively. The pump fluences are set to be 100 $\mu J/cm^2$.



https://dx.doi.org/10.1021/acs.jpca.0c08440
J. Phys. Chem. A 2020, 124, 10447−10456

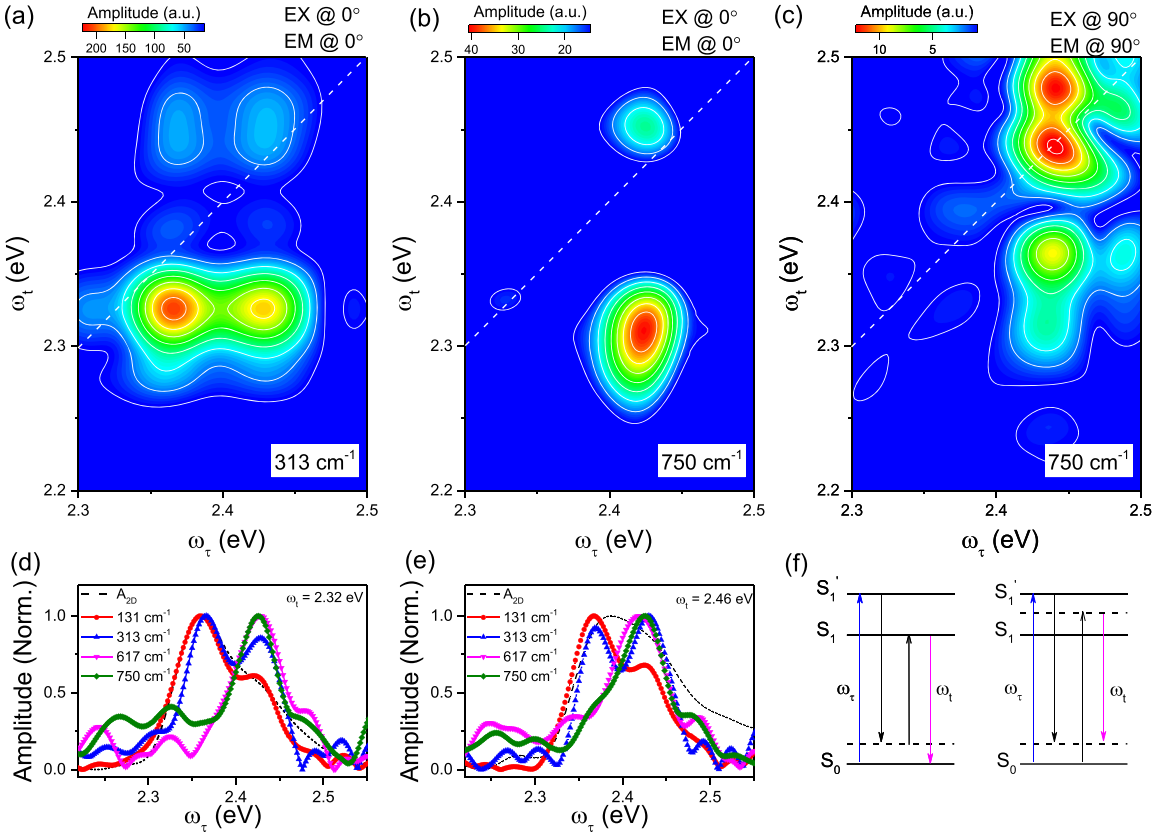


**Figure 6.** Beating maps in 2DES spectra at (a) 313 and (b) 750 $cm^{-1}$ with pump and probe beam parallel to the *b* axis. (c) Beating maps at 750 $cm^{-1}$ with pump and probe beam perpendicular to the *b* axis. Normalized spectra of the beatings versus excitation energy at different beating frequencies for the traces probed at (d) 2.32 and (e) 2.46 eV. The black dashed lines present the sliced 2D spectra at the same probe energy for comparison. (f) Excitation pathway elucidating the oscillating components in the GSB dynamics in a displaced harmonic oscillator energy level scheme. The dashed line indicates the vibrational replica of an electronic level.

$^1(T_1T_1)$ state in tetracene crystals. We speculate such a resonance is possibly caused by the presence of $^1(T_1T_1)$ states. The vibronic interaction may mix the vibrational hot $S_1$', the higher branch of Davydov $S_1$* and the $^1(T_1T_1)$ states, result in the breaking of J-aggregation behavior. The mode of 750 $cm^{-1}$ is the ring deformation mode, which is also found to be a tag for the vibrationally coherent formation of $^1(T_1T_1)$ state in the film of TIPS–tetracene.[41] Also, such a mixing behavior can well explain the ultrafast relaxation from the $S_1$* to $S_1$ states. The assignment of the $^1(T_1T_1)$ state for the abnormal beating behavior may be further examined by analyzing the modes coupled to $^1(T_1T_1)$ state both theoretically and experimentally.

The above mode analysis basically focuses on the intramolecular modes. It is argued that the intramolecular modes are particularly important in dynamically modulating the electronic coupling between LE and TT states. In the crystalline rubrene and pentacene, recent study on the coherent vibrational dynamics suggest that the conical intersection for SF dynamics is driven by some key low-frequency intermolecular modes.[38,75] In our current work, the beating spectra related to the TT states (Figure 5, part h and p), there are some signals in the low frequency regime which, however, cannot be clearly resolved from the noise level. It is valuable to further improve the measurement and combine the experiments with temperature control for future study.

## CONCLUSION

We have conducted polarization-dependent 2DES measurements on the tetracene single crystals to study the excited state specified SF dynamics. The (T···T) formation is observed to be on the time scale of 86 ps and is nearly independent of the excitation configurations. The subpicosecond dynamics and vibrational coherence have been found to be highly sensitive to the states photoexcited and probed. The mode analysis suggests that the high frequency mode is coupled to the LE and TT states which may contribute to the energy compensation. Notably, the vibrational hot $S_1$' state shows a resonance that violates the aggregation behavior, implying the mixing between LE and TT states. These findings suggest that the interplay between exciton–vibration coupling and the dipole–dipole interaction is essential for endothermic SF in molecular aggregates.

## ASSOCIATED CONTENT

### Supporting Information

The Supporting Information is available free of charge at https://pubs.acs.org/doi/10.1021/acs.jpca.0c08440.

Schematic polarization-dependent optical absorption, excitation fluence-dependent 2DES measurements, 2DES measurements with perpendicular excitation, schematic diagram of excited states dynamics, traces of triplet pair generation recorded with different excitation configurations, traces with oscillation components upon



https://dx.doi.org/10.1021/acs.jpca.0c08440
J. Phys. Chem. A 2020, 124, 10447–10456

high fluence excitation, traces and coherent phonon mode analysis with parallel excitation at 2.42 eV, and Raman spectroscopy and computation analysis of vibrational modes (PDF)

## AUTHOR INFORMATION


### Corresponding Author

**Chunfeng Zhang** − *National Laboratory of Solid State Microstructures, School of Physics, and Collaborative Innovation Center for Advanced Microstructures, Nanjing University, Nanjing 210093, P. R. China;* orcid.org/0000-0001-9030-5606; Email: cfzhang@nju.edu.cn

### Authors

**Guodong Wang** − *National Laboratory of Solid State Microstructures, School of Physics, and Collaborative Innovation Center for Advanced Microstructures, Nanjing University, Nanjing 210093, P. R. China*

**Zhixing Liu** − *National Laboratory of Solid State Microstructures, School of Physics, and Collaborative Innovation Center for Advanced Microstructures, Nanjing University, Nanjing 210093, P. R. China*

**Rui Wang** − *National Laboratory of Solid State Microstructures, School of Physics, and Collaborative Innovation Center for Advanced Microstructures, Nanjing University, Nanjing 210093, P. R. China*

**Haibo Ma** − *School of Chemistry and Chemical Engineering, Nanjing University, Nanjing 210093, P. R. China;* orcid.org/0000-0001-7915-3429

**Xiaoyong Wang** − *National Laboratory of Solid State Microstructures, School of Physics, and Collaborative Innovation Center for Advanced Microstructures, Nanjing University, Nanjing 210093, P. R. China;* orcid.org/0000-0003-1147-0051

**Min Xiao** − *National Laboratory of Solid State Microstructures, School of Physics, and Collaborative Innovation Center for Advanced Microstructures, Nanjing University, Nanjing 210093, P. R. China; Department of Physics, University of Arkansas, Fayetteville, Arkansas 72701, United States*

Complete contact information is available at: https://pubs.acs.org/10.1021/acs.jpca.0c08440


### Notes

The authors declare no competing financial interest.

## ACKNOWLEDGMENTS

This work is supported by the National Key R&D Program of China (Grant Nos. 2018YFA0209101 and 2017YFA0303700), the National Science Foundation of China (Grant Nos. 21922302, 21873047, 11904168, 91833305, and 91850105), Science and Technology Project of Jiangsu Province of China (BK20190290), the Priority Academic Program Development of Jiangsu Higher Education Institutions (PAPD), and the Fundamental Research Funds for the Central University. The authors acknowledge Dr. Xuewei Wu for providing technical assistance.

## REFERENCES


(1) Smith, M. B.; Michl, J. Singlet fission. *Chem. Rev.* **2010**, *110* (11), 6891−6936.

(2) Smith, M. B.; Michl, J. Recent advances in singlet fission. *Annu. Rev. Phys. Chem.* **2013**, *64*, 361−386.

(3) Casanova, D. Theoretical modeling of singlet fission. *Chem. Rev.* **2018**, *118* (15), 7164−7207.

(4) Rao, A.; Friend, R. H. Harnessing singlet exciton fission to break the Shockley−Queisser limit. *Nat. Rev. Mater.* **2017**, *2* (11), 1−12.

(5) Miyata, K.; Conrad-Burton, F. S.; Geyer, F. L.; Zhu, X.-Y. Triplet pair states in singlet fission. *Chem. Rev.* **2019**, *119* (6), 4261−4292.

(6) Congreve, D. N.; Lee, J.; Thompson, N. J.; Hontz, E.; Yost, S. R.; Reusswig, P. D.; Bahlke, M. E.; Reineke, S.; Van Voorhis, T.; Baldo, M. A. External quantum efficiency above 100% in a singlet-exciton-fission−based organic photovoltaic cell. *Science* **2013**, *340* (6130), 334−337.

(7) Shockley, W.; Queisser, H. J. Detailed balance limit of efficiency of p−n junction solar cells. *J. Appl. Phys.* **1961**, *32* (3), 510−519.

(8) Tayebjee, M. J.; Gray-Weale, A. A.; Schmidt, T. W. Thermodynamic limit of exciton fission solar cell efficiency. *J. Phys. Chem. Lett.* **2012**, *3* (19), 2749−2754.

(9) Hanna, M.; Nozik, A. Solar conversion efficiency of photovoltaic and photoelectrolysis cells with carrier multiplication absorbers. *J. Appl. Phys.* **2006**, *100* (7), 074510.

(10) Groff, R.; Avakian, P.; Merrifield, R. Coexistence of exciton fission and fusion in tetracene crystals. *Phys. Rev. B* **1970**, *1* (2), 815.

(11) Geacintov, N.; Pope, M.; Vogel, F. Effect of magnetic field on the fluorescence of tetracene crystals: Exciton fission. *Phys. Rev. Lett.* **1969**, *22* (12), 593.

(12) Schlosser, D. W.; Philpott, M. R. Singlet excitons in crystalline naphthalene, antracene, tetracene and pentacene. *Chem. Phys.* **1980**, *49* (2), 181−199.

(13) Wilson, M. W.; Rao, A.; Clark, J.; Kumar, R. S. S.; Brida, D.; Cerullo, G.; Friend, R. H. Ultrafast dynamics of exciton fission in polycrystalline pentacene. *J. Am. Chem. Soc.* **2011**, *133* (31), 11830−11833.

(14) Wilson, M. W.; Rao, A.; Ehrler, B.; Friend, R. H. Singlet exciton fission in polycrystalline pentacene: From photophysics toward devices. *Acc. Chem. Res.* **2013**, *46* (6), 1330−1338.

(15) Musser, A. J.; Liebel, M.; Schnedermann, C.; Wende, T.; Kehoe, T. B.; Rao, A.; Kukura, P. Evidence for conical intersection dynamics mediating ultrafast singlet exciton fission. *Nat. Phys.* **2015**, *11* (4), 352−357.

(16) Thorsmølle, V. K.; Averitt, R. D.; Demsar, J.; Smith, D.; Tretiak, S.; Martin, R.; Chi, X.; Crone, B.; Ramirez, A.; Taylor, A. Morphology effectively controls singlet-triplet exciton relaxation and charge transport in organic semiconductors. *Phys. Rev. Lett.* **2009**, *102* (1), 017401.

(17) Birech, Z.; Schwoerer, M.; Schmeiler, T.; Pflaum, J.; Schwoerer, H. Ultrafast dynamics of excitons in tetracene single crystals. *J. Chem. Phys.* **2014**, *140* (11), 114501.

(18) Piland, G. B.; Bardeen, C. J. How morphology affects singlet fission in crystalline tetracene. *J. Phys. Chem. Lett.* **2015**, *6* (10), 1841−1846.

(19) Ma, L.; Zhang, K.; Kloc, C.; Sun, H.; Michel-Beyerle, M. E.; Gurzadyan, G. G. Singlet fission in rubrene single crystal: Direct observation by femtosecond pump−probe spectroscopy. *Phys. Chem. Chem. Phys.* **2012**, *14* (23), 8307−8312.

(20) Burdett, J. J.; Müller, A. M.; Gosztola, D.; Bardeen, C. J. Excited state dynamics in solid and monomeric tetracene: The roles of superradiance and exciton fission. *J. Chem. Phys.* **2010**, *133* (14), 144506.

(21) Wilson, M. W.; Rao, A.; Johnson, K.; Gélinas, S.; Di Pietro, R.; Clark, J.; Friend, R. H. Temperature-independent singlet exciton fission in tetracene. *J. Am. Chem. Soc.* **2013**, *135* (44), 16680−16688.

(22) Tayebjee, M. J.; Clady, R. G.; Schmidt, T. W. The exciton dynamics in tetracene thin films. *Phys. Chem. Chem. Phys.* **2013**, *15* (35), 14797−14805.

(23) Zhang, B.; Zhang, C.; Xu, Y.; Wang, R.; He, B.; Liu, Y.; Zhang, S.; Wang, X.; Xiao, M. Polarization-dependent exciton dynamics in tetracene single crystals. *J. Chem. Phys.* **2014**, *141* (24), 244303.

(24) Burdett, J. J.; Bardeen, C. J. Quantum beats in crystalline tetracene delayed fluorescence due to triplet pair coherences

produced by direct singlet fission. *J. Am. Chem. Soc.* **2012**, *134* (20), 8597−8607.
(25) Jankus, V.; Snedden, E. W.; Bright, D. W.; Arac, E.; Dai, D.; Monkman, A. P. Competition between polaron pair formation and singlet fission observed in amorphous rubrene films. *Phys. Rev. B: Condens. Matter Mater. Phys.* **2013**, *87* (22), 224202.
(26) Tao, S.; Matsuzaki, H.; Uemura, H.; Yada, H.; Uemura, T.; Takeya, J.; Hasegawa, T.; Okamoto, H. Optical pump-probe spectroscopy of photocarriers in rubrene single crystals. *Phys. Rev. B: Condens. Matter Mater. Phys.* **2011**, *83* (7), 075204.
(27) Chan, W.-L.; Ligges, M.; Jailaubekov, A.; Kaake, L.; Miaja-Avila, L.; Zhu, X.-Y. Observing the multiexciton state in singlet fission and ensuing ultrafast multielectron transfer. *Science* **2011**, *334* (6062), 1541−1545.
(28) Zimmerman, P. M.; Zhang, Z.; Musgrave, C. B. Singlet fission in pentacene through multi-exciton quantum states. *Nat. Chem.* **2010**, *2* (8), 648−652.
(29) Lukman, S.; Chen, K.; Hodgkiss, J. M.; Turban, D. H.; Hine, N. D.; Dong, S.; Wu, J.; Greenham, N. C.; Musser, A. J. Tuning the role of charge-transfer states in intramolecular singlet exciton fission through side-group engineering. *Nat. Commun.* **2016**, *7* (1), 1−13.
(30) Margulies, E. A.; Miller, C. E.; Wu, Y.; Ma, L.; Schatz, G. C.; Young, R. M.; Wasielewski, M. R. Enabling singlet fission by controlling intramolecular charge transfer in π-stacked covalent terrylenediimide dimers. *Nat. Chem.* **2016**, *8* (12), 1120.
(31) Busby, E.; Xia, J.; Wu, Q.; Low, J. Z.; Song, R.; Miller, J. R.; Zhu, X.; Campos, L. M.; Sfeir, M. Y. A design strategy for intramolecular singlet fission mediated by charge-transfer states in donor−acceptor organic materials. *Nat. Mater.* **2015**, *14* (4), 426−433.
(32) Yost, S. R.; Lee, J.; Wilson, M. W.; Wu, T.; McMahon, D. P.; Parkhurst, R. R.; Thompson, N. J.; Congreve, D. N.; Rao, A.; Johnson, K.; et al. A transferable model for singlet-fission kinetics. *Nat. Chem.* **2014**, *6* (6), 492−497.
(33) Monahan, N.; Zhu, X.-Y. Charge transfer−mediated singlet fission. *Annu. Rev. Phys. Chem.* **2015**, *66*, 601−618.
(34) Chan, W.-L.; Ligges, M.; Zhu, X. The energy barrier in singlet fission can be overcome through coherent coupling and entropic gain. *Nat. Chem.* **2012**, *4* (10), 840−845.
(35) Basel, B. S.; Zirzlmeier, J.; Hetzer, C.; Reddy, S. R.; Phelan, B. T.; Krzyaniak, M. D.; Volland, M. K.; Coto, P. B.; Young, R. M.; Clark, T.; et al. Evidence for charge-transfer mediation in the primary events of singlet fission in a weakly coupled pentacene dimer. *Chem.* **2018**, *4* (5), 1092−1111.
(36) Beljonne, D.; Yamagata, H.; Brédas, J.; Spano, F.; Olivier, Y. Charge-transfer excitations steer the davydov splitting and mediate singlet exciton fission in pentacene. *Phys. Rev. Lett.* **2013**, *110* (22), 226402.
(37) Margulies, E. A.; Logsdon, J. L.; Miller, C. E.; Ma, L.; Simonoff, E.; Young, R. M.; Schatz, G. C.; Wasielewski, M. R. Direct observation of a charge-transfer state preceding high-yield singlet fission in terrylenediimide thin films. *J. Am. Chem. Soc.* **2017**, *139* (2), 663−671.
(38) Miyata, K.; Kurashige, Y.; Watanabe, K.; Sugimoto, T.; Takahashi, S.; Tanaka, S.; Takeya, J.; Yanai, T.; Matsumoto, Y. Coherent singlet fission activated by symmetry breaking. *Nat. Chem.* **2017**, *9* (10), 983−989.
(39) Tamura, H.; Huix-Rotllant, M.; Burghardt, I.; Olivier, Y.; Beljonne, D. First-principles quantum dynamics of singlet fission: Coherent versus thermally activated mechanisms governed by molecular π stacking. *Phys. Rev. Lett.* **2015**, *115* (10), 107401.
(40) Breen, I.; Tempelaar, R.; Bizimana, L. A.; Kloss, B.; Reichman, D. R.; Turner, D. B. Triplet separation drives singlet fission after femtosecond correlated triplet pair production in rubrene. *J. Am. Chem. Soc.* **2017**, *139* (34), 11745−11751.
(41) Stern, H. L.; Cheminal, A.; Yost, S. R.; Broch, K.; Bayliss, S. L.; Chen, K.; Tabachnyk, M.; Thorley, K.; Greenham, N.; Hodgkiss, J. M.; et al. Vibronically coherent ultrafast triplet-pair formation and subsequent thermally activated dissociation control efficient endothermic singlet fission. *Nat. Chem.* **2017**, *9* (12), 1205.
(42) Dover, C. B.; Gallaher, J. K.; Frazer, L.; Tapping, P. C.; Petty, A. J., II; Crossley, M. J.; Anthony, J. E.; Kee, T. W.; Schmidt, T. W. Endothermic singlet fission is hindered by excimer formation. *Nat. Chem.* **2018**, *10* (3), 305.
(43) Bakulin, A. A.; Morgan, S. E.; Kehoe, T. B.; Wilson, M. W.; Chin, A. W.; Zigmantas, D.; Egorova, D.; Rao, A. Real-time observation of multiexcitonic states in ultrafast singlet fission using coherent 2d electronic spectroscopy. *Nat. Chem.* **2016**, *8* (1), 16−23.
(44) Le, A. K.; Bender, J. A.; Arias, D. H.; Cotton, D. E.; Johnson, J. C.; Roberts, S. T. Singlet fission involves an interplay between energetic driving force and electronic coupling in perylenediimide films. *J. Am. Chem. Soc.* **2018**, *140* (2), 814−826.
(45) Schnedermann, C.; Alvertis, A. M.; Wende, T.; Lukman, S.; Feng, J.; Schröder, F. A.; Turban, D. H.; Wu, J.; Hine, N. D.; Greenham, N. C.; et al. A molecular movie of ultrafast singlet fission. *Nat. Commun.* **2019**, *10* (1), 1−11.
(46) Morrison, A. F.; Herbert, J. M. Evidence for singlet fission driven by vibronic coherence in crystalline tetracene. *J. Phys. Chem. Lett.* **2017**, *8* (7), 1442−1448.
(47) Fujihashi, Y.; Chen, L.; Ishizaki, A.; Wang, J.; Zhao, Y. Effect of high-frequency modes on singlet fission dynamics. *J. Chem. Phys.* **2017**, *146* (4), 044101.
(48) Tempelaar, R.; Reichman, D. R. Vibronic exciton theory of singlet fission. Ii. Two-dimensional spectroscopic detection of the correlated triplet pair state. *J. Chem. Phys.* **2017**, *146* (17), 174704.
(49) Tempelaar, R.; Reichman, D. R. Vibronic exciton theory of singlet fission. I. Linear absorption and the anatomy of the correlated triplet pair state. *J. Chem. Phys.* **2017**, *146* (17), 174703.
(50) Tempelaar, R.; Reichman, D. R. Vibronic exciton theory of singlet fission. Iii. How vibronic coupling and thermodynamics promote rapid triplet generation in pentacene crystals. *J. Chem. Phys.* **2018**, *148* (24), 244701.
(51) Deng, G.-H.; Wei, Q.; Han, J.; Qian, Y.; Luo, J.; Harutyunyan, A. R.; Chen, G.; Bian, H.; Chen, H.; Rao, Y. Vibronic fingerprint of singlet fission in hexacene. *J. Chem. Phys.* **2019**, *151* (5), 054703.
(52) Xie, X.; Santana-Bonilla, A.; Fang, W.; Liu, C.; Troisi, A.; Ma, H. Exciton-phonon interaction model for singlet fission in prototypical molecular crystals. *J. Chem. Theory Comput.* **2019**, *15* (6), 3721−3729.
(53) Damrauer, N. H.; Snyder, J. L. Symmetry-directed control of electronic coupling for singlet fission in covalent bis-acene dimers. *J. Phys. Chem. Lett.* **2015**, *6* (22), 4456−4462.
(54) Alguire, E. C.; Subotnik, J. E.; Damrauer, N. H. Exploring non-condon effects in a covalent tetracene dimer: How important are vibrations in determining the electronic coupling for singlet fission? *J. Phys. Chem. A* **2015**, *119* (2), 299−311.
(55) Grumstrup, E. M.; Johnson, J. C.; Damrauer, N. H. Enhanced triplet formation in polycrystalline tetracene films by femtosecond optical-pulse shaping. *Phys. Rev. Lett.* **2010**, *105* (25), 257403.
(56) Hestand, N. J.; Spano, F. C. Expanded theory of h- and j-molecular aggregates: The effects of vibronic coupling and intermolecular charge transfer. *Chem. Rev.* **2018**, *118* (15), 7069−7163.
(57) Lim, S.-H.; Bjorklund, T. G.; Spano, F. C.; Bardeen, C. J. Exciton delocalization and superradiance in tetracene thin films and nanoaggregates. *Phys. Rev. Lett.* **2004**, *92* (10), 107402.
(58) Yamagata, H.; Norton, J.; Hontz, E.; Olivier, Y.; Beljonne, D.; Brédas, J.-L.; Silbey, R.; Spano, F. The nature of singlet excitons in oligoacene molecular crystals. *J. Chem. Phys.* **2011**, *134* (20), 204703.
(59) Hybl, J. D.; Albrecht Ferro, A.; Jonas, D. M. Two-dimensional fourier transform electronic spectroscopy. *J. Chem. Phys.* **2001**, *115* (14), 6606−6622.
(60) Brixner, T.; Mančal, T.; Stiopkin, I. V.; Fleming, G. R. Phase-stabilized two-dimensional electronic spectroscopy. *J. Chem. Phys.* **2004**, *121* (9), 4221−4236.
(61) Hamm, P.; Zanni, M. *Concepts and methods of 2d infrared spectroscopy*; Cambridge University Press: 2011.

(62) Mandal, A.; Chen, M.; Foszcz, E. D.; Schultz, J. D.; Kearns, N. M.; Young, R. M.; Zanni, M. T.; Wasielewski, M. R. Two-dimensional electronic spectroscopy reveals excitation energy-dependent state mixing during singlet fission in a terrylenediimide dimer. *J. Am. Chem. Soc.* **2018**, *140* (51), 17907−17914.
(63) Cho, M. H. Coherent two-dimensional optical spectroscopy. *Chem. Rev.* **2008**, *108* (4), 1331−1418.
(64) Cundiff, S. T.; Mukamel, S. Optical multidimensional coherent spectroscopy. *Phys. Today* **2013**, *66* (7), 44−49.
(65) Jonas, D. M. Two-dimensional femtosecond spectroscopy. *Annu. Rev. Phys. Chem.* **2003**, *54*, 425−463.
(66) Zhu, W. D.; Wang, R.; Zhang, C. F.; Wang, G. D.; Liu, Y. L.; Zhao, W.; Dai, X. C.; Wang, X. Y.; Cerullo, G.; Cundiff, S.; Xiao, M. Broadband two-dimensional electronic spectroscopy in an actively phase stabilized pump-probe configuration. *Opt. Express* **2017**, *25* (18), 21115−21126.
(67) Podzorov, V. Organic single crystals: Addressing the fundamentals of organic electronics. *MRS Bull.* **2013**, *38* (1), 15−24.
(68) Kistler, K. A.; Pochas, C. M.; Yamagata, H.; Matsika, S.; Spano, F. C. Absorption, circular dichroism, and photoluminescence in perylene diimide bichromophores: Polarization-dependent h- and j-aggregate behavior. *J. Phys. Chem. B* **2012**, *116* (1), 77−86.
(69) Petelenz, P.; Slawik, M. Band-structure of charge-transfer excitons in crystalline tetracene. *Chem. Phys. Lett.* **1991**, *178* (4), 337−340.
(70) Wan, Y.; Guo, Z.; Zhu, T.; Yan, S.; Johnson, J.; Huang, L. Cooperative singlet and triplet exciton transport in tetracene crystals visualized by ultrafast microscopy. *Nat. Chem.* **2015**, *7* (10), 785−792.
(71) Cao, J.; Cogdell, R. J.; Coker, D. F.; Duan, H.-G.; Hauer, J.; Kleinekathoefer, U.; Jansen, T. L. C.; Mancal, T.; Miller, R. J. D.; Ogilvie, J. P.; Prokhorenko, V. I.; Renger, T.; Tan, H.-S.; Tempelaar, R.; Thorwart, M.; Thyrhaug, E.; Westenhoff, S.; Zigmantas, D. Quantum biology revisited. *Sci. Adv.* **2020**, *6* (14), No. eaaz4888.
(72) Monahan, N. R.; Sun, D.; Tamura, H.; Williams, K.; Xu, B.; Zhong, Y.; Kumar, B.; Nuckolls, C.; Harutyunyan, A. R.; Chen, G.; Dai, H.-L.; Beljonne, D.; Rao, Y.; Zhu, X. Y. Dynamics of the triplet-pair state reveals the likely coexistence of coherent and incoherent singlet fission in crystalline hexacene. *Nat. Chem.* **2017**, *9* (4), 341−346.
(73) Sun, K.; Huang, Z.; Gelin, M. F.; Chen, L.; Zhao, Y. Monitoring of singlet fission via two-dimensional photon-echo and transient-absorption spectroscopy: Simulations by multiple davydov trial states. *J. Chem. Phys.* **2019**, *151* (11), 114102.
(74) Zhou, N.; Chen, L.; Huang, Z.; Sun, K.; Tanimura, Y.; Zhao, Y. Fast, accurate simulation of polaron dynamics and multidimensional spectroscopy by multiple davydov trial states. *J. Phys. Chem. A* **2016**, *120* (9), 1562−1576.
(75) Duan, H.-G.; Jha, A.; Li, X.; Tiwari, V.; Ye, H.; Nayak, P. K.; Zhu, X.-L.; Li, Z.; Martinez, T. J.; Thorwart, M.; Miller, R. J. D. Intermolecular vibrations mediate ultrafast singlet fission. *Sci. Adv.* **2020**, *6* (38), No. eabb0052.


https://dx.doi.org/10.1021/acs.jpca.0c08440
*J. Phys. Chem. A* 2020, 124, 10447−10456